Smart Structures and Systems, *Vol. 27, No. 3 (2021) 407-419*
DOI: https://doi.org/10.12989/sss.2021.27.3.407

Cluster analysis and damage identification for FRP/steel-confined RC column using AE technique

Fangzhu Du [*1], Dongsheng Li [2] and Dapeng Qiu [1]

[1] *School of Civil Engineering, Shandong Jianzhu University, Jinan, Shandong 250101, China*
[2] *School of Civil Engineering, Dalian University of Technology, Dalian, Liaoning 116024, China*

(*Received March 10, 2019, Revised November 15, 2020, Accepted November 19, 2020*)

Abstract. This article presents the damage evaluation and pattern recognition for the newly proposed fiber reinforced polymer (FRP)/steel-confined reinforced concrete columns. The interaction of FRP material, steel tube, and reinforced concrete lead to complex damage mechanisms and invisible damage modes. The prevailing acoustic emission (AE) technique was applied to monitor the damage process and detect the sheltered damages under cyclic loading. Characteristic AE parameters, such as energy and duration, were extracted to disclose the damage evolution and evaluate the damage state. Three typical damage stages were identified. The fuzzy C–means (FCM) algorithm and particle swarm optimization (PSO) algorithm were applied as efficient clustering tools to discriminate different damage signals of FRP/steel-confined RC columns. Five types of damage mechanisms were identified and illustrated based on the statistical analysis of typical AE features. Furthermore, typical damage waveforms were extracted, the frequency content of each damage signal was discussed on the basis of wavelet transform.

Keywords: FRP/steel-confined RC column; acoustic emission; pattern recognition; cluster analysis; wavelet analysis

1. Introduction

Steel tube-confined reinforced concrete (STCRC) columns are proposed to improve the constraint effect and ductility of the traditional concrete-filled steel tube (CFST) columns. Liu *et al*. (2009) and Zhou *et al*. (2009) studied the mechanical behavior of STCRC columns, the steel tube in STCRC columns showed a better confinement effect and seismic behavior than that of traditional CFST column. However, steel tubes are susceptible to corrosion. Fiber-reinforced polymer (FRP) with high strength to low weight ratio, high corrosion resistance, and low thermal expansion coefficient, have been extensively used in civil engineering for strengthen purpose. Wrapping layers of FRP laminates on the surface of STCRC columns can prevent the steel tube be corroded and improve their mechanical behavior. The feasibility of FRP-steel-concrete composite structures have been reported by Huang *et al*. (2016) and Zeng *et al*. (2018). Wang *et al*. (2019, 2020) thoroughly investigated the compressive behavior and seismic performance of FRP/steel- confined RC columns under different loading conditions. However, the damage detection and evaluation have not been comprehensively interpreted.

Compared with traditional RC columns, FRP/steel-confined RC structure offer highly complex and sheltered damages by combining FRP composites, steel, and anisotropic concrete; such a structure however, makes damage recognition very cumbersome. Damages caused by concrete cracking, FRP delamination, steel deformation, and interface slipping and friction, are inevitable during the damage process of steel-confined RC columns. Therefore, developing SHM and non-destructive method for damage assessment and pattern recognition for that structure are of great significance.

Acoustic emission (AE) is a non-destructive and real-time monitoring technique that can feasibly catch the micro vibrations on the surface of materials. Compared with other non-destructive technique, AE is fast and less labor intensive. It not only can monitor damages near the sensor sites, but also can cover certain areas where excited stress waves accessible, without affecting the integrity of structures (Prem and Murthy 2016). Given its high sensitivity and precision, the AE technique has been extensively applied in civil engineering for SHM and non-destructive evaluation (NDE) purpose. For example, Aggelis *et al*. (2016) studied the damage accumulation and failure mechanisms of a reinforced concrete beam strengthened by textile reinforced cement using AE technique and digital image correlation. Ma and Li (2017) applied the AE technique to monitor and evaluate the damage levels of FRP-confined concrete columns under quasi-static loading. Li *et al*. (2015, 2017a) thoroughly investigated the AE behavior of FRP/steel-confined RC columns under different loading condition, and proposed several indicators including cumulative energy, index of damage, and b-value to trace the damage evolution and evaluate the damage state. However, the damage pattern and mechanism of the FRP/steel-confined RC columns have not been discussed elaborately.

Cluster analysis is a reliable approach for data classification and pattern recognition. Wu *et al*. (2018)

*Corresponding author, Ph.D., Professor,
E-mail: dufangzhu20@sdjzu.edu.cn

ISSN: 1738-1584 (Print), 1738-1991 (Online)

reported the damage pattern recognition of CFRP cable with a novel bonding anchorage by using the combination of unsupervised K-means clustering and supervised K-nearest neighbor classification (K-NN). Gutkin *et al*. (2011) combined the K-means and Self-organizing Map (SOM) to identify the damage pattern of CFRP laminates under different test condition. Marec *et al*. (2008) applied wavelet transform to de-noise the AE damage signals, principal component analysis (PCA) to reduce data redundancy, and the fuzzy C–means (FCM) approach to cluster the principal components into different classes. Li *et al*. (2016) applied the FCM cluster method to identify the damages of CFRP-confined circular concrete-filled steel tubular columns under monotonic loading. The particle swarm optimization (PSO) algorithm, which was developed based on the swarm behavior of fish, bees, etc, has shown great potential in global optimization in multi-dimensional space (Nickabadi *et al*. 2011). Li *et al*. (2017b) studied the stress corrosion mechanisms for steel wires through acoustic emission PSO technique. Zitto *et al*. (2015) investigated the frequency feature of AE signal generated from dynamic tests of reinforced concrete slab by continuous wavelet transform (CWT).

In the current study, the entire damage process of GFRP/steel-confined RC columns under cyclic compressive loading was monitored using the AE system. (1): Failure process and damage condition were revealed and evaluated based on the variation of characteristic AE features. (2): Damage classification was achieved by the FCM and PSO cluster operation, and the proposed statistical analysis of typical AE features promoted the identification of different damage types. (3): Typical AE signal of each damage type was extracted, and de-noised by wavelet transform, detailed frequency contents of each damage signal was also discussed.

2. Data processing algorithms

2.1 AE feature analysis

AE is a class of phenomena whereby transient elastic waves are generated through a rapid release of stored energy during material degradation and contains useful information about the damage mechanisms and fracture modes. Fig. 1 provides the typical AE waveform. AE features, such as amplitude, energy, duration, rise time, counts, intensity, and frequency are commonly extracted to analyze the micro failure mechanisms of different structures (Kumar *et al*. 2017). AE amplitude and energy are connects to cracking intensity. AE duration and frequency depend on the motion of material degradation, and carry information about the cracking mode.

2.2 Principal component analysis

Principle component analysis (PCA) is an orthogonal linear transformation that can project n-dimensional data matrix into k-dimensional space ($k < n$). It is an effective and useful multivariate analysis method which is usually used to reduce dimensionality of a large data set to enable better analysis and visualization of data (Li *et al*. 2014). The procedure of PCA can be expressed as a splitting of original data into a sum of matrix, TP^{T}, and a residual matrix E (Manson *et al*. 2001) (Eq. (1))

$$\boldsymbol{X = TP^{T} + E}, \tag{1}$$

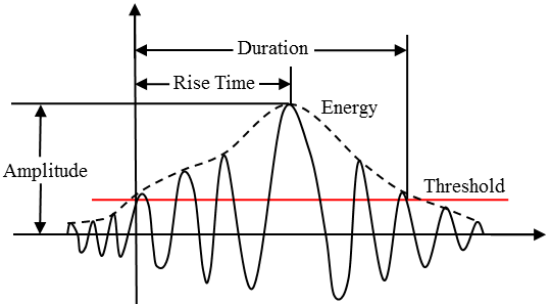

Fig. 1 Typical AE waveform

where T is the score matrix corresponding to the principal

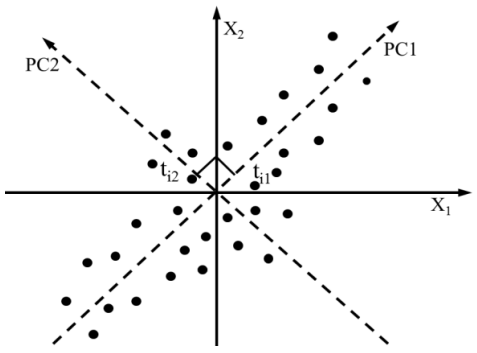

Fig. 2 Description of PCA analysis

components, P is the weight matrix containing each variable's weight vector, and E is the residual matrix.

PCA projects the input data on the new coordinates (called principal components) with maximum variance in the datasets. Based on the covariance matrix, the ordered orthogonal basis is created, with its first eigenvector having the direction of the largest variance. Fig. 2 shows the first two principal components (PC1 and PC2).

Before the PCA, sample normalization should be conducted to guarantee that all data matrices are comparable with one another. The maxima–minima value method is used in this study.

2.3 Cluster validity analysis

Various indicators, such as the Xie–Beni index (*XB*), Davies–Bouldian index (*DB*), Dunn index, and classification entropy, can be used for cluster validity analysis. In this study, the *DB* and *XB* indexes are selected to determine the optimal cluster number.

(1) *DB* (Davies and Bouldin 1979). The *DB* index checks the dissimilarity of intra cluster and inter cluster based on the inherent data set. Eq. (2) provides the mathematical formulation of *DB* index

$$DB = \frac{1}{n}\sum_{i=1}^{n} \underset{i\neq j}{max}\left(\frac{\sigma_i + \sigma_j}{d(c_i, c_j)}\right), \tag{2}$$

where n is the cluster number, σ_i represents the average distance of all nodes to its cluster center c_i (intra distance), and d (c_i, c_j) denotes the centroid distance of two different cluster (inter distance). A small *DB* index yields better clustering results.

(2) 2) *XB* (Xie and Beni 1991). The *XB* index based on the fuzzy cluster theory and defined as follows

$$XB(U,V,c) = \frac{\frac{1}{n}\sum_{i=1}^{c}\sum_{j=1}^{n} u_{ij}^{m}\left\|v_i - x_j\right\|^2}{min\left\|v_i - v_j\right\|^2} \quad (i \neq j), \tag{3}$$

where c is the cluster number, n is the object number, u_{ij} represents the membership value of the jth object belonging to the ith category, x_j represents the jth object in the ith category, and v_i is the ith cluster center. A local minimum *XB* value indicates good cluster validity.

2.4 Fuzzy C–means algorithm

The burgeoning Fuzzy C–means (FCM) cluster is advantageous over previous hard cluster methods because its fuzzy intrinsic, which permits each data point belong to a cluster specified by a membership grade, has become the most popular method for pattern recognition (Li *et al*. 2016). The target of the algorithm is to find the cluster centers C_i to minimize the feature function J (Marec *et al*. 2008).

$$J(U,V) = \sum_{j=1}^{n}\sum_{i=1}^{k}[u_i(x_j)]^f d^2(x_j, C_i), \tag{4}$$

where k is the cluster number, f is the fuzzy degree, U denotes the fuzzy membership grade matrix and V represents the matrix for cluster centers C_i. For example

$$U = \begin{bmatrix} u_1(x_1) & u_1(x_2) & \dots & u_1(x_n) \\ u_2(x_1) & u_2(x_2) & \dots & u_2(x_n) \\ \dots & \dots & \dots & \dots \\ u_k(x_1) & u_k(x_2) & \dots & u_k(x_n) \end{bmatrix}, \tag{5}$$

$$V = [C_1|C_2|\dots C_m], \tag{6}$$

d (x_j,C_i) denotes the similarity matrix between the data point x_j and its cluster center, u_i (x_j) is the membership value of jth data point to the ith cluster, under the condition

$$\sum_{i=1}^{k} u_i(x_j) = 1 \quad \forall j, \tag{7}$$

2.5 Particle swarm optimization

The emerging particle swarm optimization (PSO) is a powerful optimization technique for finding a global optimum in a multi-dimensional searching space (Qi *et al*. 2018). Given an n-dimensional space containing m particles $z = \{z_1,z_2,\dots, z_m\}$, each particle has a unique velocity denoted by $v_i = \{v_{i1}, v_{i2},\dots, v_{in}\}$ and position denoted by $z_i = \{z_{i1}, z_{i2},\dots, z_{in}\}$. The algorithm calculates the fitness of each particle. The particles adjust their location to search for a new solution through local and global extrema. During the motion, each particle records the best position referred to as P_{id} (local optimal extrema), and the overall best position referred to as P_{gd} (global optimal extrema). The position z_i (t) of each particle is updated by the recursive formula (see in Fig. 3)

$$z_{id}(t+1) = z_{id}(t) + v_{id}(t+1) \tag{8}$$

$$\begin{aligned} v_{id}(t+1) = w \cdot v_{id}(t) + \eta_1 \cdot rand_1 \cdot \left(P_{id} - z_{id}(t)\right) \\ +\eta_2 \cdot rand_2 \cdot \left(P_{gd} - z_{id}(t)\right) \end{aligned} \tag{9}$$

where v_{id} (t+1) is the updated velocity of the ith particle in dth dimension, w is the inertial weight, $rand_1$ and $rand_2$ are distinct random values in [0,1], and η_1 and η_2 are the cognition and social coefficients. In order to avoid premature convergence, a constraint on the velocity limit V_{max} of particles is generally proposed (Nickabadi *et al*. 2011).

2.6 Wavelet transform

WT decomposes a time domain signal into shifted and scaled versions of different frequency band. WT has good time resolution at high frequency band and favorable frequency resolution at low frequency band. Mathematical formulation for WT is explained as follows (Sadegh *et al*. 2016)

$$W_f(a,b) = |a|^{-\frac{1}{2}}\int_R x(t)\overline{\psi\left(\frac{t-b}{a}\right)}dt, \tag{10}$$

where a and b are the scale and position variables, which

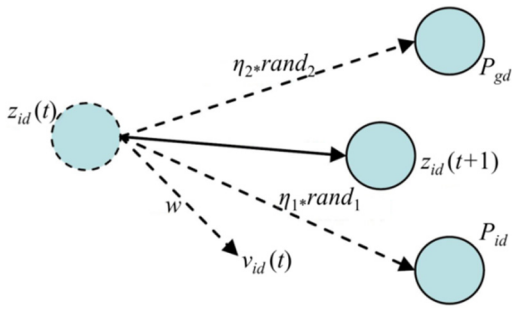

Fig. 3 Schematic of particle update

are used for scaling and shifting of the mother wavelet. $W(a,b)$ is the wavelet coefficient which indicates the correlation between signal $x(t)$ and the mother wavelet $\psi(t)$.

Specially, assign that $a = a\ j\ 0$ and $b = ka\ j\ 0b_0$, where $j \in Z$ is the decomposition level and $a_0 \neq 1$ is a constant, this is the so-called discrete wavelet transform (DWT). Mathematically describe for DWT can be expressed as

$$Wf(j,k) = a_0^{-\frac{j}{2}} \int_A x(t)\overline{\psi\left(a_0^{-j}t - kb_0\right)}\,dt. \qquad (11)$$

In wavelet analysis, a time signal can be split into a series of approximation and detail parts, the approximation part denotes the low-frequency component of the signal, whereas, the detail part represents high-frequency section.

3. Experimental procedures

3.1 Specimen fabrication

Six GFRP/steel-confined RC columns were tested with a diameter of 250 mm. Each column has a total height of 580 mm. All specimens are wrapped with four layers of GFRP cloth (0.354 mm each layer). The customized Q235 steel tube has a thickness of 2 mm. The C45 commercial concrete has a measured compressive strength of 50.2 MPa. Table 1 provides the detailed properties of the test materials. The design and manufacture of the test columns were based on the prescribed procedures of *Chinese Code for Design of Concrete Structures* (*GB50010–2010*) and *Chinese Code for design of strengthening concrete structure* (*GB50367–2013*). To avoid the GFRP/steel tube bearing axial load directly, two 10 mm circumferential loops were cut off at both end. Fig. 4 shows the construction information of test columns.

Table 1 Material properties

Material	Yield strength (MPa)	Tensile strength (MPa)	Elastic modulus (GPa)	Dimension (mm)	Elongation (%)
Steel tube	218.6	293.7	220	2	15.6
Rebar	417.0	590.7	204	14	17.5
Stirrup	323.3	565.4	217	8	18.3
GFRP cloth	/	≥ 1699.2	72	0.354	2.36
Agent	/	≥ 38	≥ 2.4	/	≥ 1.5

Fig. 4 Construction information of GFRP/steel-confined RC columns: (a) schematic diagram; (b) photograph of the test specimens; and (c) test apparatus

Table 2 Data acquisition features for the AE system

Sensor type	Peak response frequency/kHz	Threshold	Sampling rate	Sampling points	PDT/μs	HDT/μs	HLT/μs
WD	100−400	40 dB	2 MSPS	2048	300	800	1000

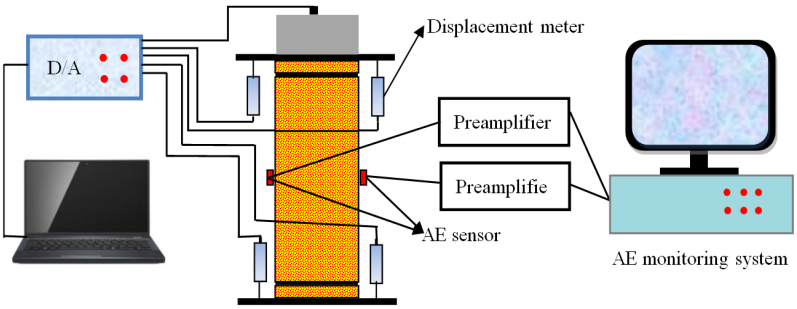

Fig. 5 Schematic of loading equipment and AE monitor system

Table 3 Basic test results of each test column

Compression specimens	Channel number	Ultimate Load/kN	Total AE hits	Compression specimens	Channel number	Ultimate load/kN	Total AE hits
CB01	1	4482	80821	CB04	1	4510	84330
	2		78954		2		82949
CB02	1	4628	85385	CB05	1	4676	87628
	2		84956		2		85570
CB03	1	4355	74855	CB06	1	4187	80141
	2		75413		2		77693

(a) (b) (c)

Fig. 6 Failure modes of test specimens: (a) after failure; (b) after strip the GFRP and steel stub; and (c) after clear the crushed concrete

3.2 Test equipment

All GFRP/steel-confined RC columns were tested at room temperature using a 10000 kN servohydraulic test machine initially controlled via an upgraded controller made by *Jinan Time Shijin Machine Group Co., Ltd*. Eight displacement meters were set to monitor the axial displacement, and cross-type electrical strain gauges were used to measure the local strain responses, as shown in Fig. 4(c). Five unloading points were evenly distributed between the yield (3500 με) and ultimate strains. The loading rate applied by displacement control was maintained for all columns to prevent its influence on damage evolution.

A two–channel MISTRAS 2001 data acquisition system manufactured by the *American Physical Acoustics Corporation* was used to record AE data during the loading

process. Two broadband AE sensors were fixed on both sides of the column symmetrically. Silicon grease was used as the coupling agent to guarantee the good workability of AE sensors. Table 2 shows data acquisition features of the AE system, and Fig. 5 shows the schematic diagram for the test equipment and AE monitoring system.

4. Damage evaluation based on AE features

In this study, characteristic AE features, including AE amplitude, counts, energy, rise time, duration, intensity, and peak frequency, were extracted during the entire loading process. The damage process was evaluated via the variation of AE features and loading history. Table 3 shows the loading capacity and AE response varied slightly among all test columns. Therefore, the CB01 was selected as the representative test specimen for further damage evaluation and pattern recognition. Fig. 6 provides the failure modes for specimen CB01, the brown rust on the surface of concrete was caused by the rusting of steel tube.

From the perspective of energy, material damage can be considered as an energy-driven instability process. Thus, AE energy can well reflect the severity of damage sources. Fig. 7 provides the loading history curve versus cumulative energy, and Fig. 8 provides the AE duration distribution. The red curve represents the loading fluctuation, while the blue curve represents the AE response. According to Figs. 7 and 8, the failure process of FRP/steel-confined RC column was divided into three distinct stages (marked by a dash line), namely the elastic stage (I), the strengthen stage (II), and the failure stage (III).

During the elastic stage, cumulative AE energy rise proportional to the increment of external load, the core RC columns bore the axial load directly. Concrete was compacted, the formation of micro-cracks result in AE hits with short duration and low energy value.

In the strengthen stage, concrete have larger radial deformation than steel tube, thereby, the FRP/steel laminates tube gradually expanded and yielded. During this stage, external load rose slowly accompanied by large plastic deformation. Meanwhile, micro cracks continuously increase. To each loading level, there was always a platform of cumulative AE energy before surpass the peak loads of last cycle, indicating the damages developed steadily. Thereafter, a large number of AE hits were recorded with high energy value and long duration, which implying more damages occurred. However, the coated GFRP/steel tube restricted the transverse expansion of core RC columns and impeded the growth of shear cracks, thus no serious damages were observed.

In the failure stage, the cumulative AE energy rapidly increases and a large number of AE hits in long duration. Correspondingly, axial load reach the peak and then gradually drop. The GFRP/steel tube and core concrete were expanded excessively, especially near the middle of the column. Fig. 6 shows the GFRP fiber were fractured and stripped and the core concrete were expanded and crushed. The increment in AE activity was mainly driven by concrete cracking, steel buckling, and FRP fracturing and peeling.

5. Damage pattern recognition based on clustering analysis

In section 4, the variation of typical AE features, such as cumulative energy and duration traced the damage evolution, evaluated the damage state, and preliminarily

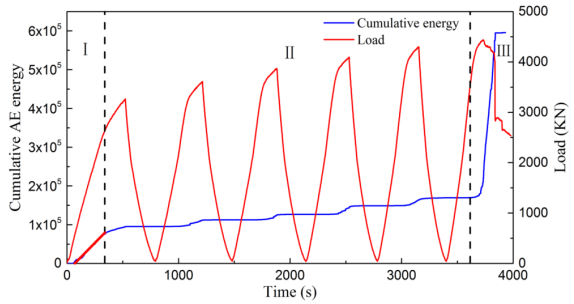

Fig. 7 Loading history versus cumulative AE energy

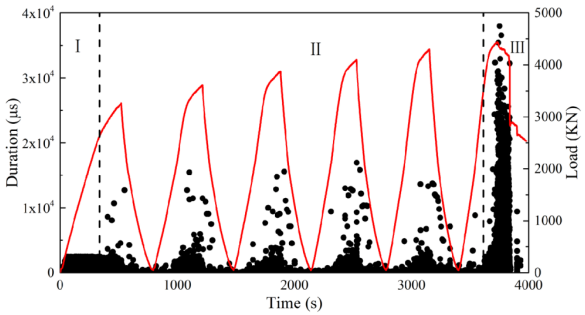

Fig. 8 AE duration-load-time distribution

disclosed the damage mechanisms. However, further investigation on damage type and mechanism are still needed, which will be discussed in this section based on the FCM cluster, PSO cluster, and statistical analysis of typical AE features.

5.1 Determination of the cluster number

Variance is the most important and commonly used indicator for measuring the dispersion degree of numerical data. In general, the characteristic variables with large variance have strong intrinsic representation ability. Thus, the maximum variance criterion have been widely applied and discussed for feature selection for data mining and machine learning (Shao and Rong 2009, Zhao *et al*. 2013). In this study, AE features including amplitude, counts, energy, rise time, duration, intensity, and peak frequency were selected based on the maximum variance criterion, which constituted the d dimensional initial data matrix. PCA was conducted to project the selected AE features into low, irrelevant dimensionality with a new coordinate system. The top three principal components were used in validity analysis and cluster analysis.

So as to guarantee the accuracy, cluster validity indicators (*DB* and *XB*) were calculated to determine the optimal cluster number (k). Fig. 9 provides the change of validity indicators (*XB* and *DB*) with the cluster number (k) range from 2 to 12. The *XB* index got a local minimum value when cluster number was 5. The *DB* index achieved a local minimum value when the cluster number was 5 and 10. In summary, both *XB* and *DB* indices reached a local minimum value when the cluster number was 5. Therefore, the optimal cluster number was determined to be 5.

5.2 Damage mechanism corresponding to cluster outcomes

In order to guarantee the reliability of cluster results, both the FCM and PSO were conducted to classify the AE signals recorded during the cyclic loading process into five representative classes. Figs. 10 and 11 provide the results of FCM cluster, and Figs. 12 and 13 provide the results of PSO results. Tables 4 and 5 provide statistical value of different AE features in FCM and PSO cluster, respectively. As shown in Figs. 10-13, the principal component (PC1 and PC2) correlogram and two-dimensional cross-plot of typical AE features distinguished the five types of damage signals effectively.

By comparison, no significant differences were observed between the results of FCM and PSO cluster (Figs. 10-13, and Tables 4-5), which means the FCM cluster also achieved global optimization as well as the PSO cluster, and both the results are reliable. The FCM and PSO algorithm mutually support better signal classification. In this section, the result of PSO cluster was discussed for further damage identification for GFRP/steel-confined RC columns.

Zitto *et al*. (2015) and Ji *et al*. (2011) reported that the damage frequency of concrete is primarily concentrated between 20 and 80 kHz. Lai *et al*. (2014) concluded that the

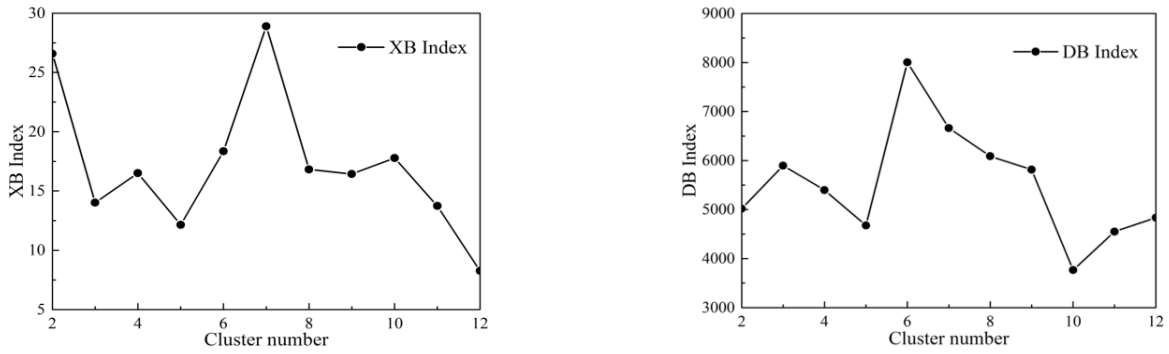

(a) (b)

Fig. 9 Cluster validity index: (a) XB index; and (b) DB index

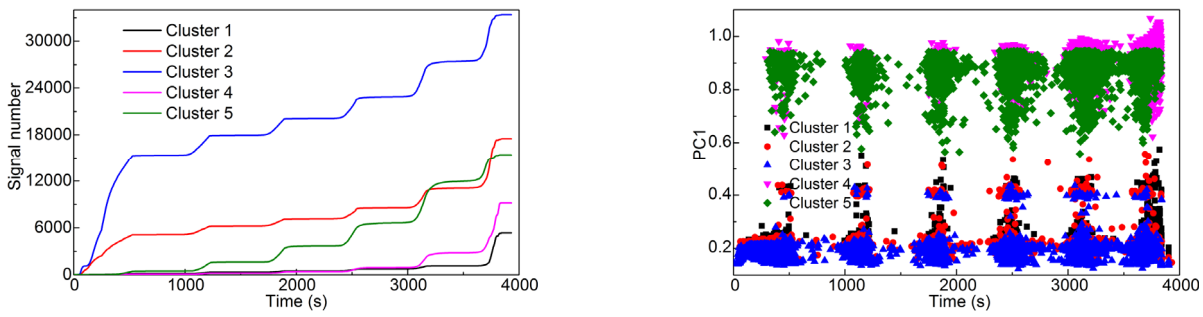

(a) (b)

Fig. 10 Time fluctuation of AE responses in FCM cluster: (a) Cumulative signal number of each cluster; and (b) PC1 distribution corresponding to time

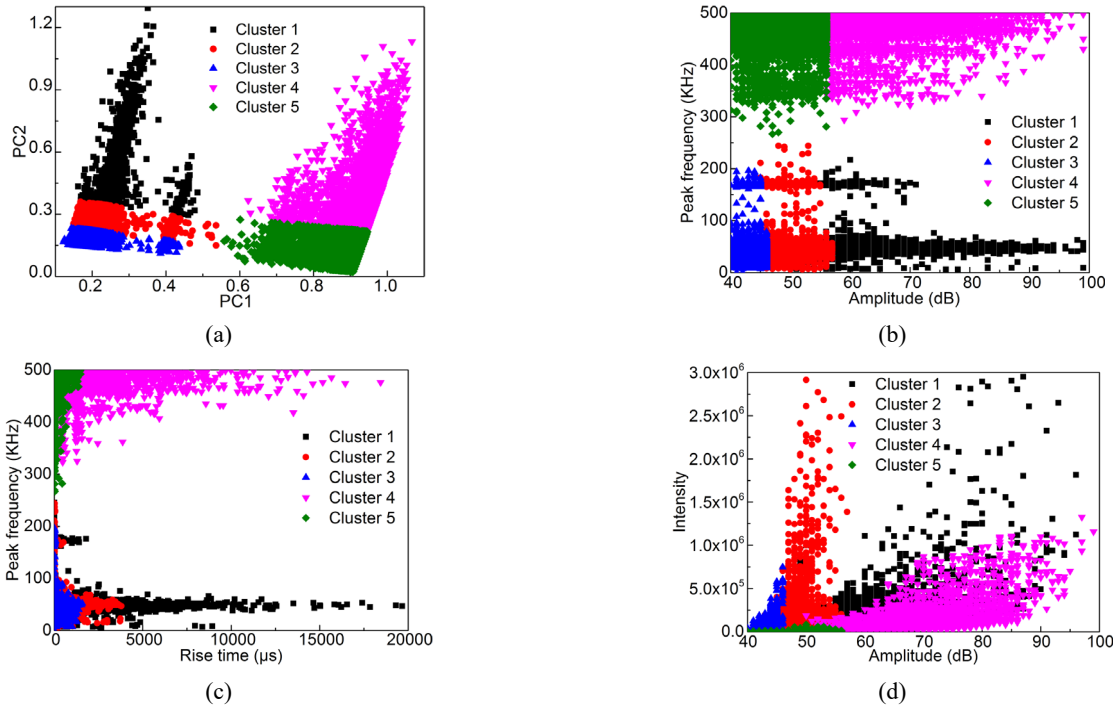

Fig. 11 Correlativity chart of AE features in FCM cluster: (a) PC1 vs. PC2 distribution; (b) amplitude vs. peak frequency distribution; (c) rise time vs. peak frequency distribution; and (d) amplitude vs. intensity distribution

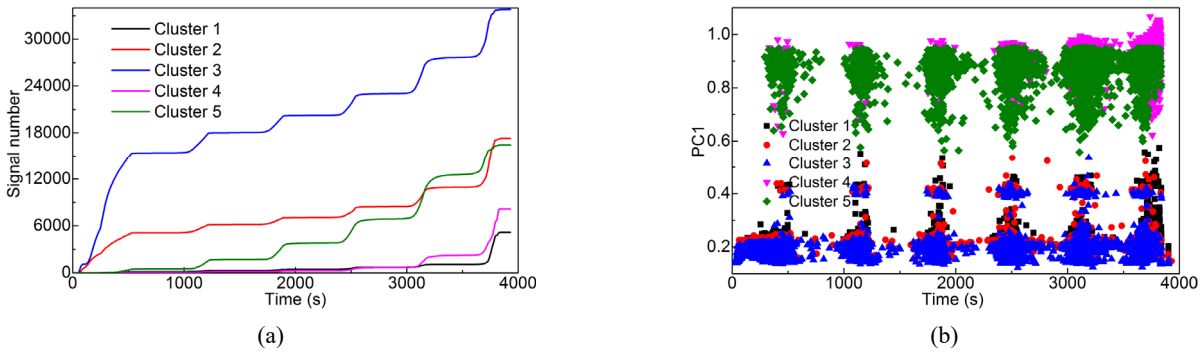

Fig. 12 Time fluctuation of AE responses in PSO cluster: (a) Cumulative signal number of each cluster; and (b) PC1 distribution corresponding to time

shear cracking and crushing of concrete are always accompanied by high AE intensity and energy dissipation. Zhang *et al.* (2013) found that the frequency of steel damages mainly ranges between 100 and 200 kHz, which is depend on different damage degree. Kadkhodapour *et al.* (2011) gave a thorough discussion on void formation, growth, and coalescence for commercial steel. Gutkin *et al.* (2011) found that the FRP matrix cracking and delaminating having frequency of 0-50 kHz and 50-150 kHz respectively, whilst, FRP breakage and fiber pull-out having peak frequency range between 400-600 kHz. Previous studies (DeGroot *et al.* 1995, Ramirez-Jimenez *et al.* 2004) also reported that the fiber de-bonding and slippage have frequency of 200-300 kHz. In addition, it is commonly granted that severe damages such as concrete crushing and FRP breakage generally have large amount of energy dissipation, accordingly, greater AE signal can be recorded.

Fig. 12 shows Clusters 1 and 4 have relatively lower signal number and were distributed in strengthen stage and failure stage; during the last few loading cycles, the signal number in Clusters 1 and 4 increased significantly. Table 5 shows that AE features, such as amplitude, rise time, counts, and energy, all in high values, indicating that Clusters 1 and 4 were caused by major damages. Moreover, Cluster 1 has low frequency of 52.86 kHz while Cluster 4 has high frequency of 477.62 kHz (Table 5). Therefore, Cluster 1 can be regard as concrete damages, including shear cracking and interpenetrating of existing cracks, and crushing of surface concrete (Fig. 14). Cluster 4 was related to major FRP damages such as fiber breakage and pull-out (Fig. 15).

Clusters 2 and 3 were continuously distributed throughout the entire damage process with a frequency of 46.70 kHz and 40.79 kHz respectively (Fig. 13 and Table 5). Cluster 3 has largest signal number but lowest AE

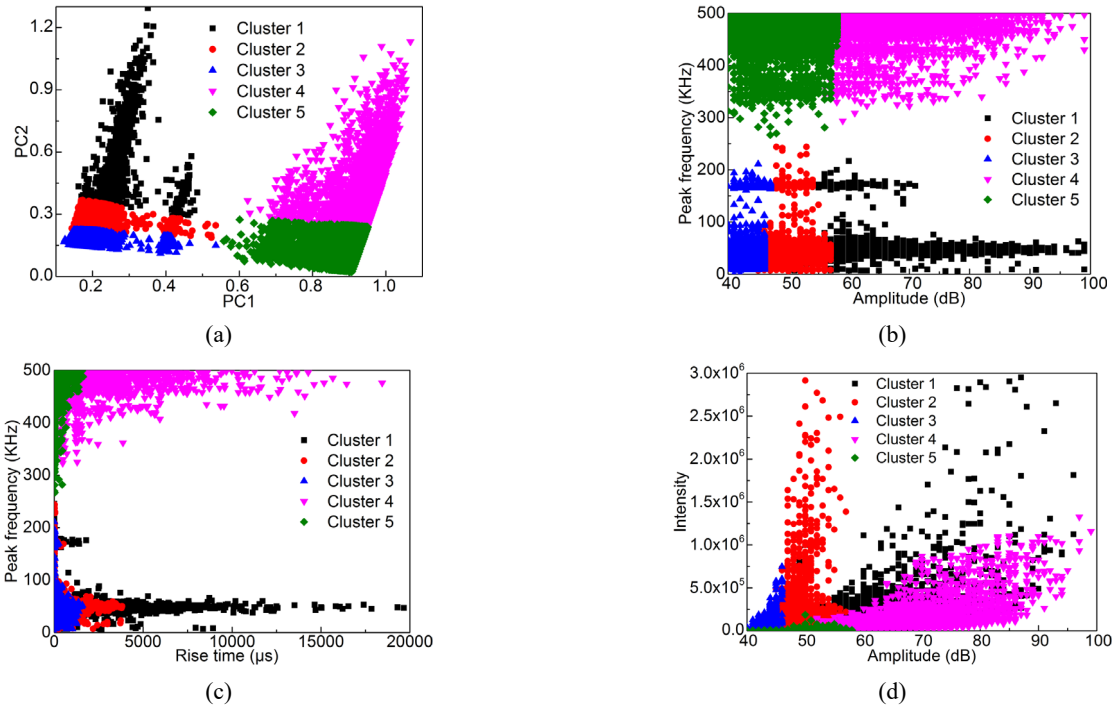

Fig. 13 Correlativity chart of AE features in FCM cluster: (a) PC1 vs. PC2 distribution; (b) amplitude vs. peak frequency distribution; (c) rise time vs. peak frequency distribution; and (d) amplitude vs. intensity distribution

Table 4 Statistical analysis of AE features for each cluster type in FCM cluster

Average AE feature	Rise time (μs)	Counts	Duration (μs)	Amplitude (dB)	Intensity	Peak frequency (kHz)
Cluster 1	1881.2	109.20	3794.9	62.94	309590.8	52.31
Cluster 2	227.71	16.72	645.73	49.46	75897.8	47.77
Cluster 3	98.64	4.55	245.46	43.00	15818.6	40.25
Cluster 4	851.43	87.01	1992.5	65.63	118938.9	478.11
Cluster 5	29.63	9.11	76.70	47.86	3290.3	427.43
Total average	316.93	24.34	762.22	49.21	57596.0	173.96

Table 5 Statistical analysis of AE features for each cluster type in PSO cluster

Average AE feature	Rise time (μs)	Counts	Duration (μs)	Amplitude (dB)	Intensity	Peak frequency (kHz)
Cluster 1	1926.3	111.96	3881.7	63.21	317901.0	52.86
Cluster 2	235.44	17.12	660.64	49.61	77501.0	46.70
Cluster 3	98.94	4.61	256.82	43.03	15807.5	40.79
Cluster 4	942.77	95.45	2204.3	66.74	132404.8	477.62
Cluster 5	35.88	9.81	91.80	48.42	3866.7	427.72
Total average	316.93	24.34	762.22	49.21	57596.0	173.96

feature values, which was primarily caused by micro damages, such as mechanical friction between the faces of FRP laminates and steel, steel and core concrete. Cluster 2 has moderate signal number and AE feature values, can be related to moderate damages such as, matrix cracking of FRP laminates, and initial cracking of concrete. Notably, there have a certain degree of mixing between Clusters 2 and 3 inevitably, because the AE features of Clusters 2 and 3 are similar.

According to Fig. 12, Cluster 5 was primarily appeared in strengthen stage and failure stage. Table 5 shows that Cluster 5 has moderate AE feature values (amplitude, rise time, counts, and energy et al.), but a high frequency of 427.72 kHz. Therefore, Cluster 5 was mostly caused by FRP damages, such as FRP laminate delaminating and de-bonding, and fiber slippage (Fig. 15).

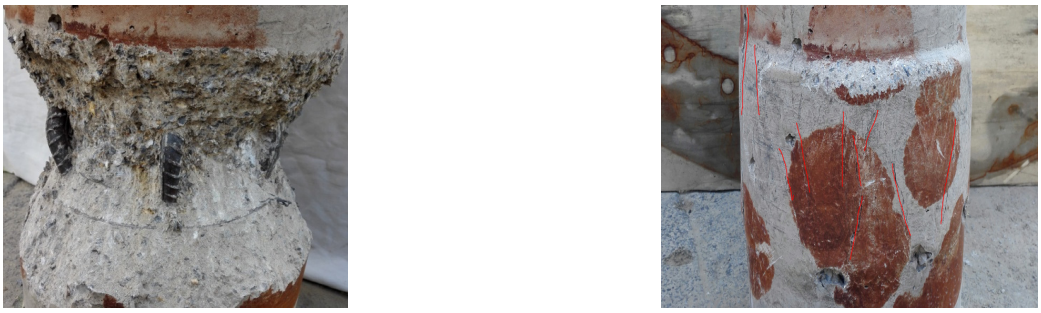

(a) (b)

Fig. 14 Typical damage modes of core RC column: (a) crushed concrete; and (b) cracked concrete

(a) (b)

Fig. 15 Typical damage modes of FRP composite and steel tube: (a) fractured and de-bonded GFRP; and (b) bucked steel tubes

In summary, typical damage modes of GFRP/steel-confined RC columns under cyclic loading were successfully identified by cluster analysis and statistical analysis. AE features, such as peak frequency and amplitude, play a major role during the pattern identification process. Most FRP damages were identified, but no steel damages were distinguished. Because most steel damages, such as initial cracking, void nucleation, and crystal dislocation motion generally generates low signal intensity, and AE sensors were mounted on the surface of FRP composite, thus, most steel damage signals were attenuated. Fig. 13 shows that there were some signals have a frequency range between 150 and 200 kHz, were caused by steel damages plausibly, however, these signals were mixed with other clusters and not separated.

6. Wavelet analysis for characteristic damage signal

In this section, typical damage signal of each damage type was extracted based on the cluster results. The discrete wavelet transform (DWT) was applied to decompose the selected damage signal into a series of details and approximations parts, using the db6 mother wavelet. Specific thresholds were assigned to each frequency band to eliminate the negative effect of noises. Then, the de-noised signal was reconstructed. The fast Fourier transform (FFT) was performed to transform the reconstructed time domain signal into frequency domain. Further investigation on its frequency content was conducted. Figs. 16-18 show the comparison for three typical raw and de-noised signals. Here, S represents the unprocessed raw signal and DS represents the de-noised signal.

Fig. 16 provides the typical signal of Cluster 1, which was caused by concrete crushing and cracking. The de-noised time domain signal was smoother and clearer. Fig. 16(b) show the frequency of Cluster 1 mainly distributed between 20 and 80 kHz. The distinct sole peak about 50 kHz has most energy contribution, implying that the peak frequency reflected the frequency content of Cluster 1 effectively.

Cluster 4 was generated by FRP fiber breakage and pull-out, Fig. 17 shows that the typical signal has a broad frequency range between 380-80 kHz. Similarly, the peak frequency of 470 kHz has most energy contribution, also reflected its frequency content.

Fig. 18 shows the frequency distribution of Cluster 5 was dispersive and complex. The main-peak was observed at approximately 380 kHz, whereas, two sub-peaks were observed at about 30 kHz (related to noises) and 410 kHz. The signal was contaminated to some extent. After wavelet reconstruction, the frequency content of 30 kHz was suppressed successfully and more energy concentrated between 300 and 500 kHz. The de-noised signal was smoother than the raw signal in both time and frequency domain. To get a better de-noise results, the reconstruction coefficient should be designed specially, and further investigation is still needed.

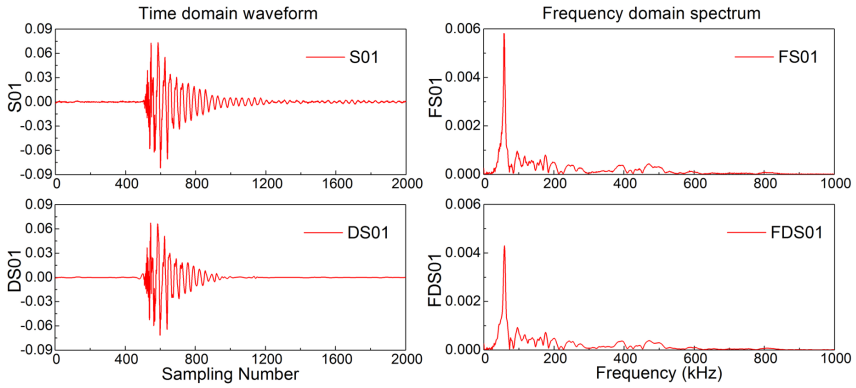

Fig. 16 Wavelet decomposition of typical damage signal in Cluster 1: (a) time domain signal; and (b) frequency domain signal

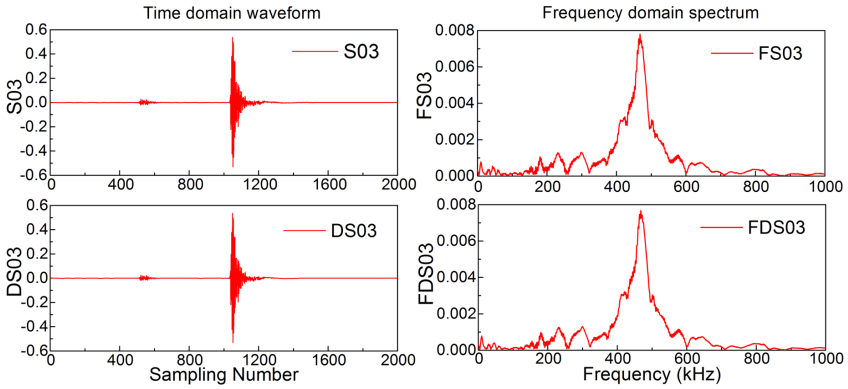

Fig. 17 Wavelet decomposition of typical damage signal in Cluster 4: (a) time domain signal; and (b) frequency domain signal

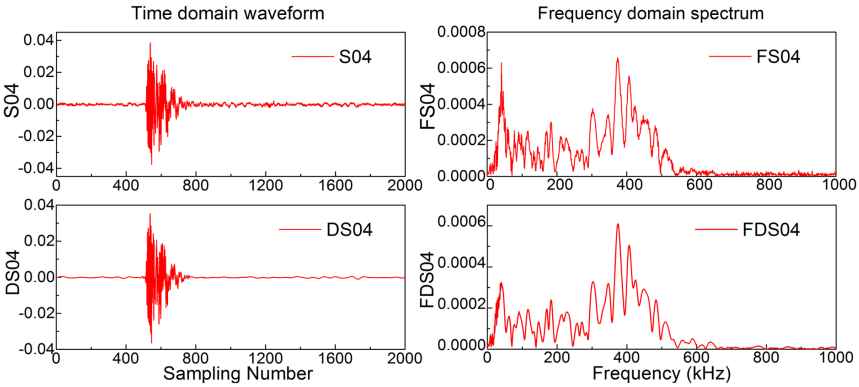

Fig. 18 Wavelet decomposition of typical damage signal for Cluster 5: (a) time domain signal; and (b) frequency domain signal

7. Conclusions

In this study, the entire damage process of FRP/steel-confined RC columns under cyclic loading was monitored using the AE technique. Damage evaluation and pattern recognition were realized based on the recorded AE signals and cluster analysis, and typical damage signals were analyzed via wavelet analysis. The major conclusions are as follows:

Typical AE features, such as cumulative energy and duration, can be used for disclosing the damage process and mechanisms for FRP/steel-confined RC structures. The damage process of test columns was evaluated into three typical stages based on AE features analysis, which was related to different damage state.

The FCM and PSO algorithms were used as efficient pattern recognition tools to discriminate the damage modes of FRP/steel-confined RC columns. These two methods mutually support better cluster results. AE amplitude and peak frequency play a major role during the pattern recognition process.

The proposed statistical analysis of typical AE features

facilitated the damage identification and mechanism illustration. Typical damage signals were decomposed and de-noised by wavelet transform, the frequency content of each damage signal was discussed detailedly.

Acknowledgments

The authors are grateful for the financial support from the National Natural Science Foundation of China (NSFC) under Grant No. 51778104, and Doctoral Research Fund Project of Shandong Jianzhu University under Grant No. X20026Z0101, and the experimental teaching lab of civil engineering of Shandong Jianzhu University.

References

Aggelis, D.G., Verbruggen, S., Tsangouri, E., Tysmans, T. and Van Hemelrijck, D. (2016), "Monitoring the failure mechanisms of a reinforced concrete beam strengthened by textile reinforced cement using acoustic emission and digital image correlation", *Smart Struct. Syst., Int. J.*, **17**(1), 91-105. https://doi.org/10.12989/sss.2016.17.1.091

Davies, D.L. and Bouldin, D.W. (1979), "A cluster separation measure", *IEEE Trans. Pattern Anal. Mach. Intel.*, **1**(2), 224-227. https://doi.org/10.1109/TPAMI.1979.4766909

DeGroot, P.J., Wijnen, P. and Janssen, R. (1995), "Real-time frequency determination of acoustic emission for different fracture mechanisms in carbon epoxy composites", *Compos. Sci. Technol.*, **55**(4), 405-412. https://doi.org/10.1016/0266-3538(95)00121-2

Gutkin, R., Green, C.J., Vangrattanachai, S., Pinho, S.T., Robinson, P. and Curtis, P.T. (2011), "On acoustic emission for failure investigation in CFRP: Pattern recognition and peak frequency analyses", *Mech. Syst. Signal Pr.*, **25**(4), 1393-1407. https://doi.org/10.1016/j.ymssp.2010.11.014

Huang, L., Yin, P., Yan, L. and Kasal, B. (2016), "Behavior of hybrid GFRP-perforated-steel tube-encased concrete column under uniaxial compression", *Compos. Struct.*, **142**, 313-324. https://doi.org/10.1016/j.compstruct.2016.02.016

Ji, H.G., Hou, Z.F., Zhang, L. and Wen, F.F. (2011), "Experimental studies on the frequency characteristics of acoustic emissions in concrete material and its dependences on strength parameters", *Appl. Acoust.*, **30**(2), 112-117.

Kadkhodapour, J., Butz, A. and Rad, S.Z. (2011), "Mechanisms of void formation during tensile testing in a commercial, dual-phase steel", *Acta. Mater.* **59**(7), 2575-2588. https://doi.org/10.1016/j.actamat.2010.12.039

Kumar, C.S., Arumugam, V., Sengottuvelusamy, R., Srinivasan, S. and Dhakal, H.N. (2017), "Failure strength prediction of glass/epoxy composite laminates from acoustic emission parameters using artificial neural network", *Appl. Acoust.*, **115**, 32-41. https://doi.org/10.1016/j.apacoust.2016.08.013

Lai, Y.S., Xiong, Y. and Cheng, L.F. (2014), "Frequency band energy characteristics of acoustic emission signals in damage process of concrete under uniaxial compression", *J. Vib. Shock*, **32**(2), 12-19.

Li, L., Lomov, S.V., Yan, X. and Carvelli, V. (2014), "Cluster analysis of acoustic emission signals for 2D and 3D woven glass/epoxy composites", *Compos. Struct.*, **116**(1), 286-299. https://doi.org/10.1016/j.compstruct.2014.05.023

Li, D.S., Chen, Z. and Feng, Q.M. (2015), "Damage analysis of CFRP-confined circular concrete-filled steel tubular columns by acoustic emission techniques", *Smart. Mater. Struct.*, **24**(8), 085017. https://doi.org/10.1088/0964-1726/24/8/085017

Li, D.S., Du, F.Z., Chen, Z. and Wang, Y.L. (2016), "Identification of failure mechanisms for CFRP-confined circular concrete-filled steel tubular columns through acoustic emission signals", *Smart Struct. Syst., Int. J.*, **18**(3), 525-540. https://doi.org/10.12989/sss.2016.18.3.525

Li, D.S., Du, F.Z. and Ou, J.P. (2017a), "Damage evaluation of fiber reinforced plastic-confined circular concrete-filled steel tubular columns under cyclic loading using the acoustic emission technique", *Smart. Mater. Struct.*, **26**(3), 035014. https://doi.org/10.1088/1361-665X/aa57c9

Li, D.S., Yang, W. and Zhang, W. (2017b), "Cluster analysis of stress corrosion mechanisms for steel wires used in bridge cables through acoustic emission particle swarm optimization", *Ultrasonics*, **77**, 22-31. https://doi.org/10.1016/j.ultras.2017.01.012

Liu, J., Zhang, S., Zhang, X. and Guo, L. (2009), "Behavior and strength of circular tube confined reinforced-concrete (CTRC) columns", *J. Constr. Steel Res.*, **65**(7), 1447-1458. https://doi.org/10.1016/j.jcsr.2009.03.014

Ma, G. and Li, H. (2017), "Acoustic emission monitoring and damage assessment of FRP-strengthened reinforced concrete columns under cyclic loading", *Constr. Build. Mater.*, **144**, 86-98. https://doi.org/10.1016/j.conbuildmat.2017.03.169

Manson, G., Worden, K., Holford, K. and Pullin, R. (2001), "Visualisation and dimension reduction of acoustic emission data for damage detection", *J. Intel. Mat. Syst. Struct.*, **12**(8), 529-536. https://doi.org/10.1177/10453890122145375

Marec, A., Thomas, J.H. and El Guerjouma, R. (2008), "Damage characterization of polymer-based composite materials: Multivariable analysis and wavelet transform for clustering acoustic emission data", *Mech. Syst. Signal Pr. Special Issue: Mechatronics*, **22**(6), 1441-1464. https://doi.org/10.1016/j.ymssp.2007.11.029

Nickabadi, A., Ebadzadeh, M.M. and Safabakhsh, R. (2011), "A novel particle swarm optimization algorithm with adaptive inertia weight", *Appl. Soft Comput.*, **11**(4), 3658-3670. https://doi.org/10.1016/j.asoc.2011.01.037

Prem, P.R. and Murthy, A.R. (2016), "Acoustic emission monitoring of reinforced concrete beams subjected to four-point-bending", *Appl. Acoust.*, **117**, 28-38. https://doi.org/10.1016/j.apacoust.2016.08.006

Qi, C., Fourie, A. and Chen, Q. (2018), "Neural network and particle swarm optimization for predicting the unconfined compressive strength of cemented paste backfill", *Constr. Build. Mater.*, **159**, 473-478. https://doi.org/10.1016/j.conbuildmat.2017.11.006

Ramirez-Jimenez, C.R., Papadakis, N., Reynolds, N., Gan, T.H., Purnell, P. and Pharaoh, M. (2004), "Identification of failure modes in glass/polypropylene composites by means of the primary frequency content of the acoustic emission event", *Compos. Sci. Technol.*, **64**(12), 1819-1827. https://doi.org/10.1016/j.compscitech.2004.01.008

Sadegh, H., Mehdi, A.N. and Mehdi, A. (2016), "Classification of acoustic emission signals generated from journal bearing at different lubrication conditions based on wavelet analysis in combination with artificial neural network and genetic algorithm", *Tribol. Int.*, **95**, 426-434. https://doi.org/10.1016/j.triboint.2015.11.045

Shao, J.D. and Rong, G. (2009), "Nonlinear process monitoring based on maximum variance unfolding projections", *Expert Syst. Appl.*, **36**(8), 11332-11340. https://doi.org/10.1016/j.eswa.2009.03.042

Wang, Y.L., Cai, G.C., Li, Y.Y., Waldmann, D., Larbi, A.S. and Tsavdaridis, K.D. (2019), "Behavior of circular fiber-reinforced polymer-steel-confined concrete columns subjected to reversed cyclic loads: experimental studies and finite-element analysis", *J. Struct. Eng.-ASCE*, **145**, 040190859.

https://doi.org/10.1061/(ASCE)ST.1943-541X.0002373
Wang, Y.L., Cai, G.C., Larbi, A.S., Waldmann, D., Tsavdaridis, K.D. and Ran, J.H. (2020), "Monotonic axial compressive behaviour and confinement mechanism of square CFRP-steel tube confined concrete", *Eng. Struct.*, **217**, 110802. https://doi.org/10.1016/j.engstruct.2020.110802
Wu, J.Y., Lan, C.M., Xian, G.J. and Li, H. (2018), "Recognition of damage pattern and evolution in CFRP cable with a novel bonding anchorage by acoustic emission", *Smart Struct. Syst., Int. J.*, **21**(4), 421-433. https://doi.org/10.12989/sss.2018.21.4.421
Xie, X.L. and Beni, G. (1991), "A validity measure for fuzzy clustering", *IEEE Trans. Pattern Anal. Mach. Intel.*, **13**(13), 841-847.
Zeng, J., Lv, J., Lin, G., Guo, Y. and Li, L. (2018), "Compressive behavior of double-tube concrete columns with an outer square FRP tube and an inner circular high-strength steel tube", *Constr. Build. Mater.*, **184**, 668-680. https://doi.org/10.1016/j.conbuildmat.2018.07.034
Zhang, Y., Zhao, G., Zhou, J. and Zhu, R. (2013), "Acoustic emission analysis of frequency characteristic for 20 # steel during tensile process", *Chem. Mach.*, **40**(5), 569-573.
Zhao, Z., Zhang, R., Cox, J., Duling, D. and Sarle, W. (2013), "Massively parallel feature selection: an approach based on variance preservation", *Mach. Learn.*, **92**(1), 195-220. https://doi.org/10.1007/s10994-013-5373-4
Zhou, X., Liu, J. and Zhang, S. (2009), "Behavior of circular tubed reinforced concrete stub columns under axial compression", *Eng. Mech.*, **26**(11), 53-59.
Zitto, M.E., Piotrkowski, R., Gallego, A., Sagasta, F. and Benavent-Climent, A. (2015), "Damage assessed by wavelet scale bands and b-value in dynamical tests of a reinforced concrete slab monitored with acoustic emission", *Mech. Syst. Signal Pr.*, **60-61**, 75-89. https://doi.org/10.1016/j.ymssp.2015.02.006

HJ